Spectromicroscopy of Poly(ethylene terephthalate): Comparison of Spectra and Radiation Damage Rates in X-ray Absorption and Electron Energy Loss

E. G. Rightor,[†] A. P. Hitchcock,*[,‡] H. Ade,[§] R. D. Leapman,[||] S. G. Urquhart,[‡] A. P. Smith,[§] G. Mitchell,[⊥] D. Fischer,[⊗] H. J. Shin,[○] and T. Warwick[#]

Analytical Sciences, B-1470, Dow Chemical, Freeport, Texas 77541, Department of Chemistry, McMaster University, Hamilton Ontario, Canada L8S 4M1, Department of Physics, North Carolina State University, Raleigh, North Carolina 27695, National Institutes of Health, BEIP, NCRR, Bethesda, Maryland 20892, Analytical Sciences Bldg. 1897, Dow Chemical, Midland, Michigan 48667, Material Science and Engineering Laboratory, National Institute of Standards and Technology, Gaithersburg, Maryland 20899, Pohang Light Source, Pohang, Korea, amd Advanced Light Source, Lawrence Berkeley National Lab, Berkeley, California 91420

Received: July 26, 1996; In Final Form: November 11, 1996[⊗]

The C 1s and O 1s X-ray absorption spectra of poly(ethylene terephthalate) (PET) have been recorded using transmission, fluorescence, and electron yield detection. The corresponding electron energy loss spectra (EELS) have been recorded in a scanning transmission electron microscope. These results are compared to the C 1s and O 1s spectra of gas phase 1,4-dimethyl terephthalate (the monomer of PET) recorded using EELS. The comparison of monomer and polymer materials in different phases and with different techniques has aided the understanding of the relative strengths and limitations of each technique as well as assisting the spectral interpretation. Good agreement is found in the overall shape and the energies of the spectral features. Relatively minor differences in intensities can be understood in terms of the properties of the individual spectroscopic techniques. The critical dose for radiation damage by 100 keV electrons incident on PET at 100 K is found to be $(1.45 \pm 0.15) \times 10^3$ eV nm^{-3}. In contrast, the critical dose for radiation damage by 302 eV X-rays incident on PET at 300 K is $(1.2 \pm 0.6) \times 10^4$ eV nm^{-3}. A figure of merit involving the product of critical energy dose and spectral efficiency (as expressed by the appropriate *G* value) is developed. This indicates that, for near-edge studies involving a 20 eV spectral width, there is ∼500-fold advantage of X-ray absorption studies on room temperature PET relative to electron energy loss studies of cooled PET.

1. Introduction

Near-edge core-excitation spectroscopy is an element specific probe of the local chemical environment of atoms in a material. Its basis is the excitation of inner-shell (core) electrons to unoccupied orbitals or bands. The core-excited state can decay by releasing X-rays (the basis for fluorescence yield (FY) detection) or by emitting Auger and secondary electrons (the basis for electron yield (EY) detection). Characterization of materials through their near-edge core-excitation spectra is useful for identifying specific functionalities in polymers,[1−4] determining the orientation of small molecules or polymers,[4,5] investigating biological systems,[6] studying the d-states in metal alloys,[7] and characterizing oxidation states in metal oxides,[8] to name just a few applications. In order to obtain optimum results, it is necessary to understand the strengths and limitations of the various methods that can be used to acquire core spectra. In polymer applications, limitations associated with radiation damage must always be considered. Core excitation in a soft X-ray microscope is particularly promising for polymer microanalysis since it has the ability to obtain high-quality spectra and images, with fewer radiation damage problems than the analogous electron-based technique. In contrast, electron microscopy techniques have the potential for achieving much higher spatial resolution but require a significantly higher radiation dose to acquire equivalent data from the same sample volume.

When core-excitation spectra are measured using X-rays as the excitation source, the technique is called near-edge X-ray absorption fine structure (NEXAFS) spectroscopy.[5] (Acronyms used in this paper are listed and defined in Table 1.) If they are measured using inelastic scattering of electrons, the technique is called electron energy loss spectroscopy (EELS). The methods are similar in that they determine aspects of the unoccupied electronic structure as sampled by core excitation, but they differ in the ways that the core-excited state couples to the incident probe and to the chosen detection methodology. These differences give rise to advantages and limitations for each technique.

The true X-ray absorption spectrum of a material is determined by measuring the incident and transmitted flux through a suitably thin sample (typically ∼0.1 μm at the C 1s edge and ∼0.5 μm at the O 1s edge for PET). NEXAFS can also be measured with electron yield detection (denoted EY-XAS) in which case the spectra are rather surface sensitive (∼1−5 nm sampling depth for $h\nu$ < 1000 eV). Fluorescence yield detection (denoted FY-XAS) can also be used. It has a much greater sampling depth (∼100 nm at 200−500 eV), and thus it is more sensitive to the bulk properties. Both EY-XAS and FY-XAS are based on recording signals associated with secondary processes. Thus, if the Auger/fluorescence branching ratio

* Corresponding author.
[†] Dow Chemical, Bldg, B-1225.
[‡] McMaster University.
[§] North Carolina State University.
[||] National Institutes of Health.
[⊥] Dow Chemical, Bldg. 1897.
[⊗] National Institute of Standards and Technology.
[○] Pohang Light Source.
[#] Lawrence Berkeley National Labs.
[⊗] Abstract published in *Advance ACS Abstracts,* February 1, 1997.

S1089-5647(96)02274-2 CCC: $14.00

TABLE 1: Acronyms

acronym	meaning
ALS	Advanced Light Source (Berkeley, CA)
DMT	dimethyl terephthalate
EELS	electron energy loss spectra
EHMO	extended Hückel molecular orbital
EICVOM	equivalent ionic core virtual orbital model
EY-XAS	electron yield X-ray absorption spectroscopy
fwhm	full width at half-maximum
FY-XAS	fluorescence yield X-ray absorption spectroscopy
ISEELS	inner-shell electron energy loss spectra
LCAO	linear combination of atomic orbitals
NEXAFS	near-edge X-ray absorption fine structure
NSLS	National Synchrotron Light Source (Brookhaven National Lab, NY)
PET	poly(ethylene terephthalate)
STEM	scanning transmission electron microscope
STXM	scanning transmission X-ray microscope
STEM-EELS	electron energy loss spectrum recorded in a STEM
STXM-XAS	X-ray absorption spectrum recorded in a STXM
VMO	virtual molecular orbital

changes for different electronic states, this would cause differences between EY or FY and the true absorption spectra.

By using highly monochromatic and intense synchrotron radiation sources, NEXAFS spectra can be recorded in moderately short acquisition times (several tens of seconds). The dependence of transition intensities on the polarization of the radiation also allows determination of the orientation of anisotropic systems, such as aligned polymers[3,9] or molecular species on surfaces.[5] Transmission X-ray spectromicroscopies have been developed recently which allow measurement of NEXAFS spectra on a submicron scale and the generation of chemically sensitive images with spatial resolution approaching 50 nm,[10] as well as the determination of the average orientation of specific functional groups with a similar resolution.[11]

The primary process in EELS is inelastic scattering of a monoenergetic electron beam by a gas or solid target. It can be used to study atoms or molecules in the gas phase (inner-shell EELS or ISEELS) with moderate (∼0.6 eV fwhm[12]) to high (<0.1 eV fwhm[13]) spectral resolution. EELS can also be recorded in a transmission electron microscope (TEM) with the potential advantage that exceptionally high spatial resolution (∼1 nm) can be achieved.[14,15] Appropriately thin (∼0.1 μm) sections of materials can be prepared by various methods and studied with STEM-EELS. Early STEM-EELS studies of polymers were limited by the high electron beam damage associated with the long recording times required by serial detectors. However, recently developed parallel-detection electron energy loss spectrometers[16] allow radiation sensitive polymers to be studied at much lower electron dose, as previously described for PET,[17,18] polyurethane model polymers,[19] polycarbonates and poly(methyl methacrylate) (PMMA).[20] The combination of STEM-EELS studies of polymers with studies of small molecule analogues using ISEELS and extended Hückel molecular orbital (EHMO) calculations has greatly aided the interpretation of the near-edge spectra of the polymers.[17,18,21]

Each of these techniques has advantages and limitations for studying polymers. We have explored these by an in-depth, multitechnique study of poly(ethylene terephthalate) (PET), a ubiquitous polymer often found in packaging applications, and a small molecule analogue, 1,4-dimethyl terephthalate (DMT), which is the repeat unit of PET. The basis for the use of small molecule (in this case monomer) species as standards for polymer spectra has been discussed and demonstrated previously.[1,17−19,21] The combination of these techniques to study PET and DMT has helped further elucidate assignments for the spectral features of the polymer and monomer. Extended Hückel (EHMO) calculations of DMT are also used to aid interpretation of transitions in the C 1s near edge region. Radiation damage is a concern with both STEM-EELS [22−24] and STXM-XAS[6] of polymers. We have made a quantitative study of radiation damage to PET in both the spatially resolved EELS and transmission XAS experiments.

2. Experimental Section

The PET sample (density of 1.385 g/cm^3) was obtained from Scientific Polymer Products. For the FY-XAS and EY-XAS measurements it was dissolved in hexafluro-2-isopropanol (Kodak) to make a 0.01% solution which was spun-cast onto a single-crystal Si wafer which had previously been coated with 20 nm of Au. For the scanning transmission X-ray microscopy (STXM) experiments the sample was microtomed at room temperature to prepare sections of ∼0.1 and ∼0.5 μm thickness.

2.1. X-ray Absorption of PET. The EY-XAS and FY-XAS experiments were performed on the U1A beam line of the National Synchrotron Light Source (NSLS) at Brookhaven National Laboratory (BNL). The apparatus has been described previously.[4,25] The X-ray monochromator slits were such that the resolution at 300 eV was 0.6 eV full width at half-maximum (fwhm). The spectra were measured by both total fluorescence yield (FY) using a gas ionization detector operating in proportional mode[26] and by partial electron yield (EY) using a channeltron detector with a bias on the entrance cone of −150 eV relative to the sample substrate. The NEXAFS spectra of PET were collected with the sample at room temperature. All NEXAFS spectra were normalized to the incident photon flux by dividing by the Io spectrum measured as the total EY from a clean gold mesh placed before the sample.

At the C 1s edge the EY-XAS technique is best done on reasonably thin films (<100 nm) in order to minimize charging effects. For FY-XAS thicker films can be used since charging does not affect the detected signal. However, films that are thicker than several absorption lengths can give rise to distorted FY-XAS spectra on account of self-absorption of the fluorescence X-rays. The distortions in FY-XAS can be minimized by using grazing takeoff detection. The absorption length is inversely related to the transition intensity (oscillator strength). For intense features, such as the C 1s $\rightarrow \pi^*$ peak of unsaturated species, the path length for 2 optical density (OD) units is ∼80 nm, and thus sections less than 0.1 μm are required to measure spectra without absorption saturation effects. (One OD corresponds to a transmitted intensity of 1/e that of the incident intensity.) At the O 1s edge the absorption length and thus the optimal thickness increase to ∼500 nm.

STXM-XAS measurements were made on room temperature samples both at the X-1A beamline at NSLS[27,28] and at beamline 7.0 at the Advanced Light Source (ALS).[29] In both systems the soft X-rays are focused by a Fresnel zone plate. The present generation of zone plates produces a spot about 50 nm fwhm in size. The flux transmitted through a thin sample is detected with a gas flow counter. For imaging, the transmission is recorded as a function of sample position by mechanically raster scanning the sample in the focal plane under computer control. Alternatively, the photon beam is left on the same sample position while the photon energy is scanned to acquire a spectrum. The natural logarithm of the ratio of the transmitted (I_t) to the incident (I_0) intensity yields the NEXAFS spectrum in true absorption mode. For this work the I_o signal was obtained from a separate normalization scan recorded without a sample (typically through a hole in the thin film). Generally, data are acquired with an energy resolution of about 0.3 eV

(NSLS) or 0.1 eV (ALS). Acquisition time is typically less than 1 min per scan.

The energy scale for the C 1s NEXAFS spectrum was calibrated at the NSLS STXM using the C 1s → 3s Rydberg peak of CO_2 at 292.8 eV,[30] generated by admixing CO_2 with the He in the microscope enclosure. The calibrated position of the main $\pi^*_{C=C}$ peak of PET is 284.8(1) eV. The 0.1 eV error estimate is associated mainly with uncertainties in a small correction required for nonlinearity of the NSLS photon energy scale. This amounted to 0.2 eV in the 8 eV difference between the energies of the π^* peaks in PET and CO_2. The π^* energy for PET is in agreement with that of 284.86(6) eV for the main $\pi^*_{C=C}$ peak in the ISEELS of DMT. The O 1s NEXAFS spectra were placed on an absolute scale by setting the main O 1s → π^* feature to 531.5 eV, the value obtained from the calibrated ISEELS spectrum of DMT.

2.2. Electron Energy Loss of 1,4-DMT. The gas phase ISEELS spectrometer has been described previously.[12] Spectra were recorded using a final electron energy of 2.5 keV, scattering angle 2°, and a resolution of 0.6 eV fwhm. Under these conditions electric dipole transitions dominate. Small angle rather than zero degree scattering is used in order to prevent the main electron beam from entering the analyzer and creating a large background. The solid DMT sample was introduced from a small metal cell directly attached to the collision cell. 1,4-DMT was obtained from Aldrich (stated purity >99%). Absolute energy scales were determined by recording spectra of a mixture of DMT and CO_2. The gas phase spectra were converted to an absolute oscillator strength scale using standard methods[31] based on background subtraction and normalization of the continuum intensity to atomic oscillator strengths.[32]

In order to present the C 1s spectra of the polymer and molecule from each technique on a common intensity scale, all of the spectra have been processed by subtracting a linear or polynomial background extrapolated from the signal below 283 eV and then setting the intensity at 300 eV to 0.0134 eV^{-1}. For the C 1s spectra the normalization was carried out at 300 eV rather than at higher energy where the continuum shape is more atomic-like, because 300 eV is below the onset of the plural scattering which distorts STEM-EELS spectra at higher energies. Similarly, the O 1s spectra have been background subtracted and normalized to the intensity at 545 eV to 0.0081 eV^{-1}.[32] As at the C 1s edge, the normalization is carried out at rather lower energy than is normally the case,[31] in order to allow comparison to the STEM-EELS data without significant intensity distortion associated with the plural scattering signal which begins around 550 eV.

2.3. Electron Energy Loss of PET. The STEM-EELS spectra were recorded using a scanning transmission electron microscope (STEM, VG Microscopes model HB501) equipped with a field emission source and a parallel detection electron spectrometer (Gatan Model 666).[33,34] The vacuum in the region of the specimen was $<5 \times 10^{-9}$ mbar. Specimens were cooled to 100 K during analysis in order to minimize radiation damage. The spectrometer collection semiangle (α) was 20 mrad while the probe convergence semiangle (β) was 3 mrad. Suitable areas for analysis were selected at low electron dose (<10 e^- nm^{-2}) using the annular dark field image. By measuring the fraction of transmitted electrons that suffered no energy loss,[14] the regions of the PET sample used for TEM-EELS analysis were estimated to be 1.0−1.5 mean free paths or 100−150 nm thick. Spectra were acquired from 5 to 10 μm square regions by rastering the defocused 100 nm probe diameter beam while recording the spectrum. In order to achieve optimal energy resolution, it was necessary to descan movement of the spectrum over the detector by applying a synchronized voltage to the spectrometer drift tube.[35] Spectra were normalized by subtracting the dark current and dividing by the spectrometer gain at each channel. The instrumental energy scale of STEM-EELS is not accurate due to power supply drifts. For this reason the main π^* feature was calibrated to the NEXAFS of PET (for the C 1s) or the ISEELS of DMT (for the O 1s). In order to isolate the individual C 1s and O 1s core loss spectral signal, an AE^{-r} background (with A and r as adjustable parameters) was subtracted.

Spectral distortion associated with plural scattering can be a problem if the sample is too thick. As noted earlier,[17] sample thickness does not affect the near- edge fine structure in PET provided that the sample is thinner than one inelastic mean free path. With thicker samples plural scattering transfers intensity from the lower energy C 1s (O 1s) → π^* bands to the region above 295 eV (550 eV), where it distorts the spectral normalization. The region of the PET sample used for the STEM-EELS measurements had a thickness of about 1.3 inelastic mean free paths, based on analysis of the low loss spectrum. From the known density of 1.385 g/cm^3 and the previously determined value for total inelastic cross section per unit mass,[36] the inelastic mean free path in PET for 100 keV incident electrons is estimated as 100 nm. Thus, we estimate the PET sample to be 130 nm thick. Due to plural scattering the S/B ratio at the carbon 1s edge drops by a factor of ~5 as the specimen increases to 1.3 inelastic mean free paths.[37] Thus, plural scattering partly accounts for the lower π^*/σ^* intensity ratio observed in the STEM-EELS spectra. Fourier ratio deconvolution[14] by the low loss spectrum recorded under similar conditions provides an accepted means to correct for plural scattering. It reduces distortion of spectral shapes and increases the π^*/σ^* intensity ratio. In addition, deconvolution provides a modest enhancement in energy resolution. For these reasons all of the STEM-EELS spectra presented in this paper have been deconvoluted using low loss spectra.

2.4. Computational Procedures. Spectral assignments have been assisted by comparisons to semiempirical extended Hückel molecular orbital (EHMO) calculations[38,39] of 1,4-DMT. The molecular geometry (C_{2h} symmetry) was obtained from an *ab initio* geometry optimization performed with a 3-21G* basis set. This calculated structure is similar to the solid state crystal structure of 1,4-DMT,[40] except that the lowest energy gas phase structure is planar whereas the methyl ester groups are nonplanar by ~5° in the solid state. The procedures used to apply EHMO to core-excitation spectroscopy have been documented in earlier studies of organometallic,[41−43] conjugated organic,[44] and polymer analogue molecules.[18,21]

Predictions of core-excitation spectra were generated from the EHMO output using the equivalent ionic core virtual orbital model (EICVOM)[45] procedures described previously.[18,43,44] Briefly, a calculation is performed on a singly charged molecule in which the core-excited atom is replaced with the $Z + 1$ atom; for example, the C 1s spectrum of the ring-substitutional site of DMT (denoted C 1s(C−R)) is derived from the EHMO calculation for singly charged DMT, modified by replacing the substituted ring carbon with a N atom. The energies of virtual molecular orbitals (VMO) of this EICVOM species are assumed to be related to the position of the core-excitation spectral lines.

Plots of the individual virtual molecular orbitals for DMT are generated in which the radii of circles about individual atoms are proportional to the $2p_z$ orbital contribution to the π^* MOs, as listed in the complete charge matrix given in the EHMO output.[44] These plots indicate the spatial distribution of the

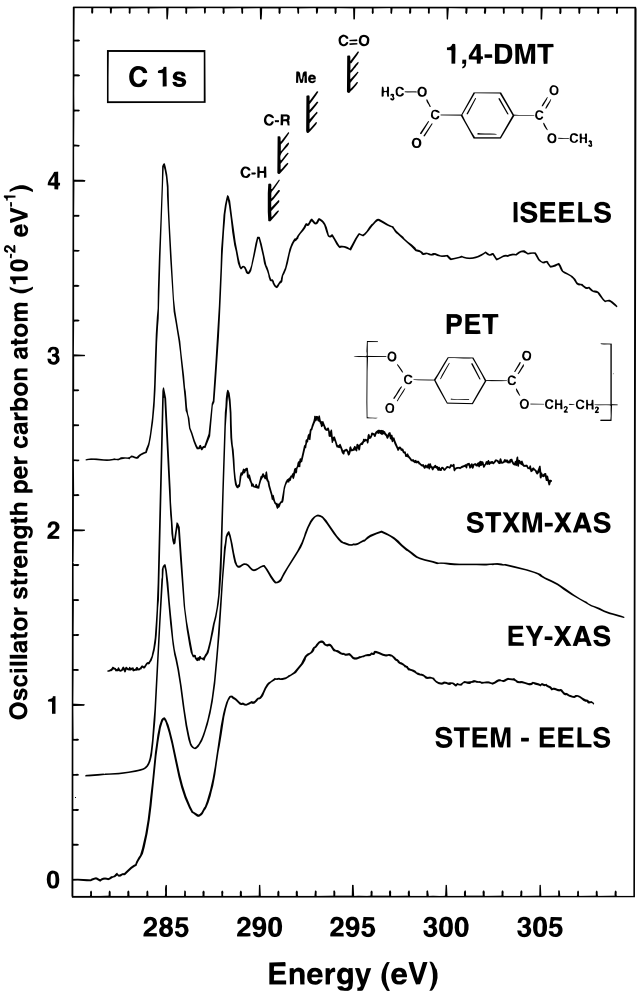

Figure 1. Comparison of as-recorded C 1s spectra of poly(ethylene terephthalate) (PET) recorded by STEM-EELS in a transmission electron microscope, EY-XAS at glancing incidence on a PET film deposited on a Si wafer, and transmission through a 200 nm thick film in the NSLS scanning transmission X-ray microscope (STXM-XAS). The PET results are compared to the C 1s spectrum of 1,4-dimethyl terephthalate (1,4-DMT), recorded in the gas phase by ISEELS using dipole-dominated scattering conditions (2800 eV impact energy, 2° angle). In each case the as-recorded spectra have been subjected to a background subtraction and normalized at 300 eV to the same oscillator strength value (0.0134 eV^{-1}). Offsets are used for clarity. The hatched lines indicate estimated core level ionization potentials of DMT.

molecular orbital in the core-excited species. They are related to the experimental spectra since the area of the circles on the core-excited atom are proportional to the square of the LCAO coefficient and thus are a measure of the intensity of the core → VMO transition.[44] These plots are very helpful in relating spectral features to structural aspects of the molecule and in visualizing the effect of core hole relaxation on particular orbitals by comparison to the same orbital in the ground state.[18,21]

3. Results and Discussion

3.1. Technique Comparison. *3.1.1 Carbon 1s Spectra of PET.* Figure 1 plots the C 1s spectra of PET recorded using electron energy loss (STEM-EELS), X-ray absorption with electron yield detection (EY-XAS), and true absorption (STXM-XAS recorded at NSLS), all in comparison with the C 1s spectrum of DMT recorded in the gas phase by ISEELS. The EY-XAS spectrum was collected at the so-called "magic" angle (55°) where orientation effects are minimal. Ouchi et al.[9a] and Lippitz et al.[9b] have recently published detailed studies of the polarization dependence of the C 1s spectrum of biaxially stretched, aligned PET. For this PET material, the intensities of specific transitions change dramatically with angle between the incident X-ray beam and the sample. The lowest energy π^* bands (all those below 290 eV) all exhibit a linear dichroism effect that is opposite to that of the three broad σ^* bands above 290 eV, consistent with the assignments we are proposing. In general, the assignments given by Ouchi et al.[9a] are similar but less detailed than those discussed in this paper. Lippitz et al.[9b] provide an in-depth discussion of the spectral features. Their polarization dependence observations fully support the assignments proposed earlier[18] and in this work. In our study the EY-XAS of the PET films spun-cast on Si showed an angular variation of less than <5% (spectra not shown). This indicates the PET molecules in our films are mainly randomly oriented, as was found by Lippitz et al.[9b] in their studies of spun-cast amorphous PET.

Overall, there is very good agreement of the major features of the PET spectra recorded by all techniques, including the FY-XAS spectrum (not shown). The similarity of the STEM-EELS spectrum to the NEXAFS spectra demonstrates that, at low dose levels, the fine structure of polymer EELS spectra corresponds well with that in spectra obtained where radiation damage is of lesser concern (ISEELS, NEXAFS). There is also generally close agreement between the spectra of PET and DMT. These C 1s spectra are similar to those of several simulations derived from the spectra of small molecule analogues of PET (see Figure 12 of ref 18). DMT is a good model for PET since its structure is very close to that of the monomer repeat unit of PET. The main difference is replacement of two C−H bonds in DMT with a C−C bond in PET. This change should make little difference to the C 1s spectrum since the change is to only a small portion of the whole repeat unit, and it occurs in a region where the perturbation is expected to be localized and thus have minimal influence on the more highly structured electronic transitions associated with the unsaturated parts of the molecule.

Differences in the resolution provided by the various techniques are responsible for a large part of the differences in these spectra. The NEXAFS spectrum of PET, recorded in the NSLS STXM with about 0.3 eV resolution, displays additional features, in particular a fully resolved peak at 285.6 eV. This feature is detected as a shoulder in the EY-XAS and in the ISEELS of DMT (both recorded with 0.6 eV fwhm resolution), but it is not detected in the STEM-EELS spectrum. In principle, it is possible to achieve 0.3 eV fwhm at the zero-loss peak in STEM-EELS with a field emission gun in a dedicated scanning transmission electron microscope.[33] However, this requires very low beam current which does not provide adequate signal in the core-excitation spectral region. For practical inner-shell studies higher beam current and larger analyzer acceptance angles are used, which degrade the energy resolution of STEM-EELS. In this work the measured fwhm of the zero-loss peak was ∼0.45 eV, but the resolution achieved at the C 1s edge is clearly worse. When the STXM-XAS spectrum of undamaged PET is convoluted with a 1.2 eV Gaussian, it is a good match to the STEM-EELS spectrum. This suggests the effective resolution of the STEM-EELS is ∼1.2 eV. From subsequent studies at least some of the resolution degradation appears to have been caused by not fully compensating for beam movement on the detector during the descanning procedure. In any case, the net result is that the 285.6 eV peak, which is seen as a clear shoulder in the ISEELS of DMT and EY-XAS of PET (0.6 eV fwhm) and a fully resolved signal in the STXM (0.3 eV fwhm), is not at all visible in STEM-EELS. In addition, several transitions are clearly resolved between 288 and 290 eV in the

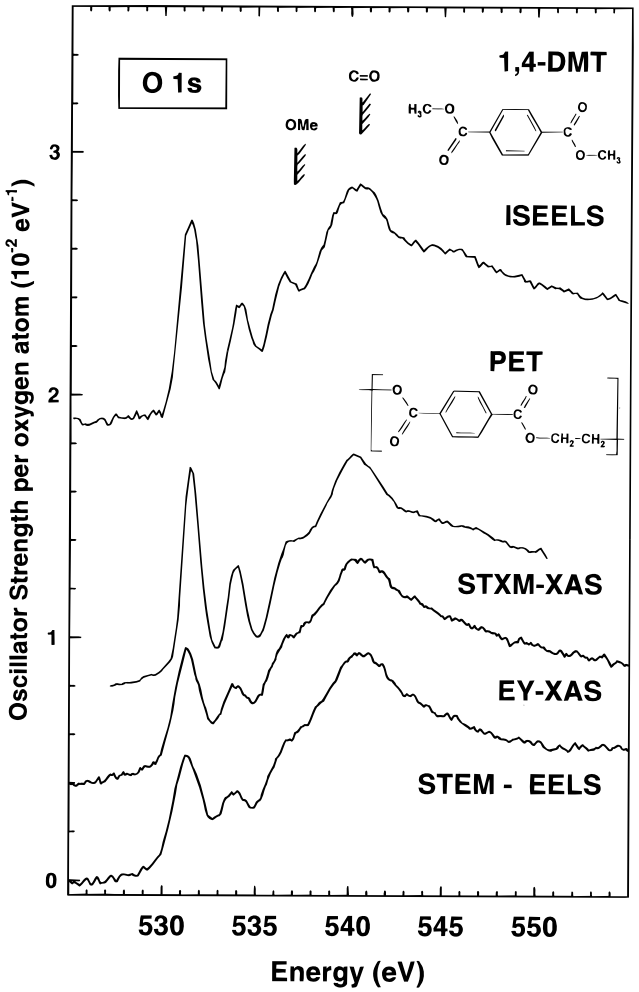

Figure 2. Comparison of the O 1s spectra of PET recorded by STEM-EELS, glancing incidence EY-XAS; and transmission in the ALS STXM. The Figure also plots the O 1s spectrum of 1,4-DMT, recorded in the gas phase by dipole-regime ISEELS. In each case the as-recorded spectra have been subjected to background subtraction and normalized at 545 eV to the same oscillator strength value (0.0081 eV^{-1}). Offsets are used for clarity. The hatched lines indicate estimated core level ionization potentials of DMT.

STXM and EY-XAS spectra of PET but appear at best as shoulders in the STEM-EELS of PET. Interestingly, when the STXM spectrum of radiation damaged PET (see section 3.2 and Figure 4) was resolution broadened, it was not possible to get adequate agreement with the STEM-EELS spectrum on account of the new transition at 286.7 eV. This is further evidence that the STEM-EELS spectrum differs from the STXM spectrum simply because of reduced resolution and not on account of radiation damage.

NEXAFS and ISEELS spectroscopy can achieve high spectral resolution, with many published examples of C 1s spectra showing spectral features with less than 0.1 eV fwhm.[13,30] Comparison of lower and higher resolution spectra can provide insights into the presence and identity of shoulders in the lower resolution results. In the case of STEM-EELS, this can provide guidance for further minimization of troubling artifacts (e.g., source instabilities, magnetic fields, radiation damage, etc.). Better understanding of these issues will facilitate the use of characteristic core-edge transitions in STEM-EELS to help identify components in polymer blends, where the high spatial resolution and numerous other imaging and microanalysis methods provide a valuable complement to EELS.

3.1.2. Oxygen 1s Spectra of PET. Figure 2 compares the O 1s spectra of PET, measured by STEM-EELS; EY-XAS; and STXM-XAS (at the ALS), all in comparison with the O 1s spectrum of DMT, measured in the gas phase by ISEELS. As at the C 1s edge, the O 1s spectra also show strong similarities in shape and number of transitions. Again, there are some resolution differences among the techniques, but the details of the O 1s spectra are less dependent than the C 1s spectra on the technique used. This is due to less spectral overlap at the O 1s edge because the natural line width is larger and the transitions are more widely spaced since there are only two different oxygen environments, as opposed to four different carbon environments. The resolution of STEM-EELS is sufficient to visualize all of the weaker transitions at higher energy than the main O 1s $\rightarrow \pi^*_{C=O}$ transition. The similarity in shape of all the spectra in Figure 2 demonstrates that there was relatively little radiation damage during acquisition of these spectra. This was particularly a concern since the STEM-EELS acquisition time for the O 1s spectrum is about 5 times longer than that for the C 1s edge.

3.2. Radiation Damage Effects. Radiation damage can be a significant concern with both electron and photon impact based core excitation studies of polymers. Electron beam induced damage of various organic and inorganic materials has been reviewed recently.[22,46] The nature and rate of damage is strongly dependent on the polymer being studied. Radiation damage induces chemical transformations (mainly reductions) and, in extreme cases, results in mass loss. These changes can be monitored by the decrease in the intensities of the spectral transitions associated with the chemically modified functional group(s). In addition, one may observe new spectral features associated with the products of radiation damage (e.g., the appearance of $\pi^*_{C=C}$ signal in radiation-damaged saturated systems). In PET the carbonyl bond is the most sensitive to radiation so carbonyl-related features are expected to be most affected. Radiation-modified spectra were recorded in both STEM-EELS and STXM-XAS measurements, and critical doses were determined. The critical dose is that dose at which the intensity of a specific spectral feature decreases to 1/e of its original value.[14,22] *In order to achieve meaningful analytical results with either technique, it is essential to use doses significantly lower than the critical dose for the specific polymer system under investigation.* Thus, we have determined critical doses for radiation damage of PET in both STEM-EELS and STXM.

3.2.1. STEM-EELS: Damage with 100 keV Electron Impact. Figure 3 shows the first four in a series of STEM-EELS spectra of PET as a function of electron dose. Changes in the spectra are noticeable, but compared to saturated polymers[46,47] the changes with the indicated beam doses are slight. This is likely due to the stabilizing effect of delocalization by the aromatic ring. As the dose increases, the intensity of the C 1s(C−H) $\rightarrow$ $\pi^*_{C=C}$ transition (285 eV) diminishes slightly while the intensity of the C 1s(C═O) $\rightarrow \pi^*_{C=O}$ transition at 288 eV decreases more noticeably. In addition, a new signal appears at 286.7 eV. The 286.7 eV signal is visible only as a shoulder in STEM-EELS but it is a well-defined peak in the STXM-XAS of radiation-damaged PET (Figure 4). These observations suggest that the mechanism of damage involves minimal ring disruption and more substantial modification in the ester groups, as expected from other studies.[46−48]

The top two panels of Figure 3 plot the background-subtracted intensities of the $\pi^*_{C=C}$ (285.0 eV) and $\pi^*_{C=O}$ (288.5 eV) features as a function of accumulated radiation dose (*d*). These results are taken from an exposure series extending well beyond that of the spectra shown in the lower panel of Figure 3. The

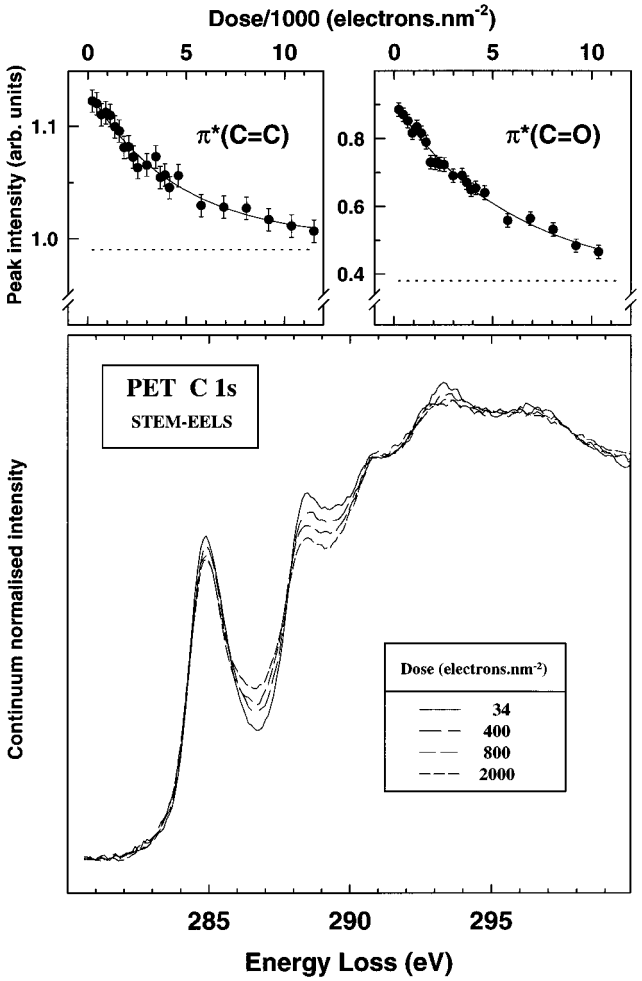

Figure 3. Dependence of the C 1s STEM-EELS spectrum of PET on the accumulated electron dose. The main panel presents the first four spectra recorded in the damage sequence. The spectra were background subtracted and normalized to a common intensity difference between 280 and 293 eV. The two top panels plot the intensity at 285 eV ($\pi^*_{C=C}$) and 288 eV ($\pi^*_{C=O}$) as a function of integrated electron dose. The solid lines are exponential fits from which the critical doses were derived. The dashed lines indicate the I_∞ values derived from the exponential fit.

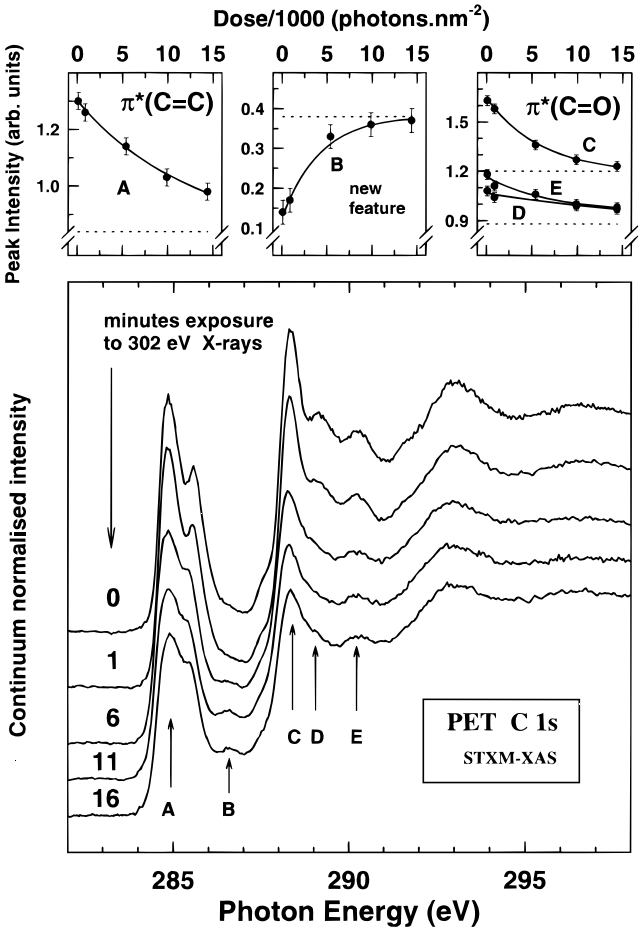

Figure 4. Dependence of the C 1s STXM-XAS spectrum of PET on the accumulated dose of 302 eV X-rays. The spectra were background subtracted and normalized to a common intensity jump between 280 and 295 eV. The top three figures plot the changes in the intensity at 285 eV ($\pi^*_{C=C}$), 286.7 eV (new damage-related feature), and the three peaks in the 288 eV ($\pi^*_{C=O}$) region, as a function of integrated X-ray dose. The solid lines are exponential fits from which the critical doses were derived. The dashed lines indicate the I_∞ values derived from the exponential fit.

characteristic critical doses are derived by fitting these curves to[14]

$$I(d) = Ae^{d/d^*} + I_\infty$$

where I_∞ is the signal after the damage has ended (at low temperature, the main effect is chemical transformation rather than mass loss), A is an intensity scale factor, and d^* is the characteristic critical dose. The characteristic critical doses derived from the dose dependence of the $\pi^*_{C=C}$ and $\pi^*_{C=O}$ signals are summarized in Table 2. The average value of 5400 electrons/nm^2 corresponds to a charge dose of 0.086 C/cm^2. Since the film thickness of 130 nm corresponds roughly to one inelastic mean free path, on average each 100 keV electron passing through the sample will be inelastically scattered once, with a mean energy loss of 35 eV.[22] Thus, the average critical dose for reduction of the $\pi^*_{C=C}$ and $\pi^*_{C=O}$ intensities is equivalent to a critical *energy* dose of $(1.9 \pm 0.2) \times 10^5$ eV nm^{-2} or $(1.45 \pm 0.15) \times 10^3$ eV nm^{-3}. The charge dose (0.086 C/cm^2) is almost an order of magnitude larger than that of 0.01 C/cm^2 for loss of crystallinity in poly(butylene terephthalate), reported by Kumar and Adams.[47] This is consistent with radiation affecting conformation and packing to a greater extent than chemical change. The critical energy dose we find for PET is similar to the values of $(2.6 \pm 0.7) \times 10^5$ eV nm^{-2} or $(6.5 \pm 1.7) \times 10^3$ eV nm^{-3}, derived by Payne and Beamson[48] from critical doses of $(1.7-2.7) \times 10^4$ electrons nm^{-2} determined by TEM-EELS for a 40 nm thick specimen of polyether ether ketone (PEEK). There was a range because the critical dose varied with the current density. Payne and Beamson predict the upper limit of usable current density is 5.8×10^3 electrons nm^{-2} s^{-1}, which they suggest will limit practical TEM-EELS studies of PEEK to areas greater than 140^2 nm^2.[48]

Our study shows that, although the EELS spectra recorded in the early stages are obtained at a small fraction of the critical dose and thus are characteristic of undamaged PET, measurements on the same region over a longer period result in readily detectible changes in the near-edge transitions of PET. Relative to previous STEM-EELS studies of PET,[17,18] distortions associated with radiation damage are lower due to use of several techniques (cryogenic cooling and beam rastering) aimed at providing the lowest possible dose while still getting good signal/noise (S/N). There is good agreement between the edge shape in the first STEM-EELS spectrum of PET and that of the EY-XAS spectrum of PET (Figure 1), after taking resolution differences into account. This agreement strongly supports the argument that at very low dose STEM-EELS spectra can be obtained which truly reflect the chemical structure of PET.

TABLE 2: Summary of Critical Dose (particles/nm^2) and Critical Energy Dose (eV/nm^2 or eV/nm^3) for Radiation Damage of PET Caused by 100 keV Electron Impact and 302 eV Photon Impact

a. 100 keV Electron Impact[a]

feature	energy (eV)	critical dose (electrons nm^{-2})	D_E/area (eV nm^{-2})	D_E/volume (eV nm^{-3})
$\pi^*_{C=C}$	285.0	$4.8(3) \times 10^2$ [b]	$1.7(2) \times 10^5$	$1.3(1) \times 10^3$
$\pi^*_{C=O}$	288.5	$6.0(3) \times 10^2$	$2.1(2) \times 10^5$	$1.6(1) \times 10^3$

b. 302 eV Photon Impact[c]

feature	energy (eV)	critical dose (photons nm^{-2})	D_E/area (eV nm^{-2})	D_E/volume (eV nm^{-3})
A. $\pi^*_{C=C}$	284.8	11780	$3.5(5) \times 10^6$	$1.7(2) \times 10^4$
B. new feature	286.7	3500	$1.0(2) \times 10^6$	$5.2(5) \times 10^3$
C. $\pi^*_{C=O}(1)$	288.2	5435	$1.5(2) \times 10^6$	$7.7(8) \times 10^3$
D. $\pi^*_{C=O}(2)$	289.1	6490	$1.8(3) \times 10^6$	$9.0(12) \times 10^3$
E. $\pi^*_{C=O}(3)$	290.1	14500	$4.3(9) \times 10^6$	$2.1(5) \times 10^4$

[a] Derived from a series of STEM-EELS recorded from PET at 100 K. The measured sample thickness was 130 nm. The beam was rastered over an area of 10×10 μm. The dose rate based on 35 eV average energy loss per 100 keV incident electron was $\sim$6 eV nm^{-3} s^{-1}. The G value for a 20 eV band at the C 1s edge is 0.0057 based on calculated energy loss cross sections of 100 keV electrons in atomic carbon[14] and the experimental angular scattering range. [b] Error derived from the quality of the exponential fit. [c] Derived from alternating higher intensity exposure and spectral scans of room temperature PET. The sample thickness was 200 nm as derived from the absorption coefficient at 310 eV. The beam was $\sim$500 nm in diameter for both exposure and spectral acquisition. The dose rate from the experimental absorptivity was $\sim$22 eV nm^{-3} s^{-1}.

Although radiation damage is far lower with the current version of parallel detection spectrometers for STEM-EELS and with the use of cryogenic techniques, one must always verify that radiation dose is not playing a role during each study. Comparison with other near-edge techniques can be helpful in this regard. This comparison of techniques demonstrates the value of using alternative techniques such as NEXAFS, and ISEELS of molecular analogues, to verify STEM-EELS results on certain polymers and to understand the magnitude and mechanism of radiation damage.

3.2.2. NEXAFS: Damage with 302 eV Photon Impact. In order to assess radiation damage with soft X-rays, PET was exposed to high radiation dose with the NSLS STXM. Figure 4 plots a sequence of five NEXAFS spectra recorded with about 0.3 eV energy resolution from a $\sim$500 nm diameter region, recorded after successive exposures of this region to monochromated 302 eV photons. The beam intensity was intentionally increased 8-fold during the radiation damage exposure by increasing the slit width and then decreased for spectral acquisition. Based on a film thickness of 200 nm (evaluated from the optical density) and a beam diameter of 500 nm, the analyzed volume is 3.9×10^7 nm^3. During radiation exposure, the transmitted intensity at 302 eV was about 200 kHz (detected by single photon counting). The optical density for the sample was 1.7 at 302 eV. Taking into account the estimated detector efficiency of 30%, the detected flux corresponds to 2.9×10^6 photons/s absorbed in the irradiated volume. Thus, the dose rate per unit area was 2.9×10^6photons s^{-1}/2.0×10^5 nm^2 or $\sim$15 photons nm^{-2} s^{-1}, or in terms of dose per unit volume, it was $2.9 \times 10^6/3.9 \times 10^7$ nm^3 or $\sim$0.08 photons nm^{-3} s^{-1}. The upper three panels of Figure 4 plot the intensity of five spectral features ($\pi^*_{C=C}$ at 284.9 eV, the new signal at 286.7 eV, and the three $\pi^*_{C=O}$-related peaks around 288 eV) as a function of accumulated dose. The critical doses derived from the fit to the intensity decay or growth curves vary between 3 500 and 14 500 photons nm^{-2} (see Table 2). This rather large spread in the critical doses may not reflect the true variation in damage rates at different chemical sites since peak heights rather than peak areas were used in the analysis, and there are definitely radiation-induced changes in peak shape. For X-ray absorption all of the photon energy is deposited into the sample. Thus, the critical dose averaged over all features is $\sim(8 \pm 4) \times 10^3$ photons nm^{-2}, which corresponds to an average *critical energy dose* of $\sim(1.2 \pm 0.6) \times 10^4$ eV nm^{-3}.

In principle, the changes of the spectra with radiation dose can provide useful information about the radiation chemistry. Detailed NEXAFS studies of radiation damage of poly(methyl methacrylate) (PMMA)[49−51] and poly(lactides)[51] indicate that, in these species, loss of carbonyl functionality is accompanied by formation of C═C bonds. Qualitatively, the relative changes in peak area (see Figure 4) indicate that the carbonyl group of PET is more susceptible to radiation damage than the phenyl ring. Based on the spectral changes, the damage is localized in the region of the carbonyls and could involve expulsion of CO or CO_2. This would explain the decrease in $\pi^*_{C=O}$ (288−290 eV), the decrease/change in $\pi^*_{C=C}$ (285−286 eV), the appearance of the 286.7 eV peak (tentatively attributed to the C 1s(O−CH═CH−O) $\rightarrow$ $\pi^*_{C=C}$ transitions in the damage product), and eventual mass loss. The surprisingly small difference in damage rates between the aromatic π^* and carbonyl π^* signals in PET may be due to stabilization of the carbonyl group by extensive delocalization onto the phenylene in PET. Further high-resolution core-excitation and infrared spectral studies on heavily radiation-damaged PET may help identify the product(s) and mechanism(s) of damage.

Clearly, it is possible to damage PET with monochromated X-rays—in fact, the extent of spectral change is much larger in Figure 4 than in Figure 3. At the same time, STXM-XAS spectra of PET with S/N ratios only slightly worse than the ones presented in Figure 4 can be recorded under full-focus conditions (i.e., on 50 nm diameter regions) in less than 30 s, so useful results can be obtained without significant radiation damage. In cases where the ultimate spatial resolution is not required, the beam can be defocused, thus allowing longer exposure times before damage occurs. The critical dose of $\sim$12 000 eV nm^{-3} for PET measured in this study is much larger that the critical dose of 63 eV nm^{-3} for PMMA measured by Zhang et al.,[49] also using the NSLS STXM. Given that PMMA is much more radiation sensitive than PET, the 200-fold difference in critical energy dose is plausible.

3.2.3. Relative Capabilities of STEM-EELS versus STXM-XAS for Analysis of Radiation Sensitive Materials. How do these measured rates for electron and photon damage of PET compare? Superficially, when one directly compares the critical dose figures in terms of integrated flux of incident particles per unit area ($\sim$5400 electrons nm^{-2} vs $\sim$8000 photons nm^{-2}), it appears that the situation is only slightly more favorable for photoabsorption than for STEM-EELS. However, the informa-

TABLE 3: Energies (eV) and Proposed Assignments of C 1s Spectral Features of Poly(ethylene Terephthalate) (PET) and-1,4-Dimethyl terephthalate (DMT)

	energies (eV)					assignment		
	PET				1,4-DMT			
no.	FY-XAS	EY-XAS	STXM	STEM-EELS	ISEELS	C−H(ring)	C−R(ring)	C═O
1	(284.8)	(284.8)	284.8(1)[a]	(284.8)	284.86(6)[b]	$\pi^*_{C=C}$ (f)[c]		
2	285.7	285.7	285.6	285.8	285.7	$\pi^*_{C=C}$ (g)	$\pi^*_{C=C}$ (d)	
3 sh			287.5		287.4		$\pi^*_{C=C/C=O}$ (e)	
4	288.1	288.2	288.2	288.5	288.2			$\pi^*_{C=O}$(+) (a)
5	289.1	289.0	289.2	289.0	289.1	$\pi^*_{C=C/C=O}$		
6	289.9	290.0	290.1	289.7	289.9		$\pi^*_{C=C/C=O}$	$\pi^*_{C=O}$(−) (b)
IP[d]					290.5	IP		
IP[d]					291.0		IP	
7 sh	291.4	291.4	291.5		291.7			
IP[d]					292.6	IP(CH_3)		
8	292.8	292.8	293.0	293.1	292.8	σ^*_1[e]		$\pi^*_{C=O}$(mix) (c)
IP[d]					294.9			IP
9	296.3	296.1	296.5(3)	296.3	296.3	σ^*_2[e]		
10	303	303.2(5)	303.5(5)	304(1)	304(1)		$\sigma^*_{C=O}$	

[a] STXM calibration: −8.0(1) eV relative to C 1s → 3s ($\upsilon = 0$) transition in CO_2 (292.8 eV[30]). Note that this uncertainty includes a contribution from nonlinearity in the photon energy scale. [b] Calibrated relative to CO_2 (−5.88(6) eV relative to π^* of CO_2 (290.74 eV)[59]). [c] These letters refer to the results of EHMO calculations (Figure 5). [d] Estimated from the IPs of related species.[53] [e] σ^*_1 and σ^*_2 refer to the characteristic C 1s continuum resonances of phenyl rings.

tion derived from each particle interaction as well as the damage caused by a 100 keV electron and a 302 eV photon are not the same. Radiation damage is generally believed to be related to energy absorbed per unit volume, and thus one should compare critical energy doses (eV nm^{-3}) not simply the critical integrated flux of incident particles. The critical energy dose for electrons and X-rays might be expected to be similar, unless there is a strong dependence of the damage on the size of energy quanta, the dose rate, or the environment of the specimen. In fact, the critical energy doses we have measured 1450 eV nm^{-3} for STEM-EELS and ∼12 000 eV nm^{-3} for STXM-XAS—differ by almost an order of magnitude. The dose rates are rather similar: ∼6 eV nm^{-3} s^{-1} for STEM-EELS and ∼22 eV nm^{-3} s^{-1} for STXM-XAS. Thus, the ∼8-fold higher critical energy dose for X-rays suggests that beam damage associated with a given dose of high-energy (inner-shell) quanta, including the secondary effects associated with the core hole decay products, is significantly less than that associated with an equivalent dose of medium-energy (valence ionization) quanta. As a caution, we note that the STEM-EELS measurements were made with the sample at liquid nitrogen temperature in a vacuum, whereas the STXM-XAS measurements were made with the sample at room temperature in 1 atm of helium. It is likely that the differences in both sample temperature and thermal conductivity to the local environment play important roles in the radiation damage rates. The derived critical energy doses for STEM-EELS of cooled PET are most likely much larger than the values for STEM-EELS of room temperature PET. There are currently several efforts underway to develop cryo-STXM, which would bring the benefits of reduced sample temperature to STXM studies of polymers. In addition, the high thermal conductivity of the He atmosphere in the STXM could help to minimize thermal damage.

In both the STXM-XAS and STEM-EELS measurements the exposure and damage assessment are largely independent of each other. In each case the critical dose was derived from the flux of incident particles and absorbed or scattered particles, not from the flux of detected particles. In addition, the critical dose was calculated from changes of spectral intensities that were significantly larger than the S/N and that do not depend on energy resolution or S/N, at least to first order. Thus, these derived critical doses are independent of instrumental factors such as resolution or spectral quality. Rather, they describe the physics of the damage, electrons versus photons. Hence, these results can be used to evaluate the relative merits of these two techniques as real analytical tools in terms of the dose necessary to get a spectrum of a certain quality.

One major difference between electron and photon impact is that each absorbed X-ray photon gives the desired spectral information whereas most of the inelastically scattered electrons excite or ionize valence electrons rather than promote core electrons. (The ratio of core to valence cross section is about 0.01.[22]) Thus, it is not surprising that the photoabsorption process is more efficient in terms of core excitation. Since the S/B is similar in both cases, with ideal detectors and spectrometers, *the critical energy dose multiplied by the efficiency for generating a spectrum of a specified spectral width* can be used as a *figure of merit* which reflects the relative capabilities of the two techniques for spatially resolved microanalysis of polymers. The spectral efficiency is expressed in STEM-EELS in terms of the *G* value, which is the amount of signal of interest generated per 100 eV of energy absorbed. If one defines the region of interest as a 20 eV band at the C 1s edge (a width which contains most of the near-edge fine structure), then the *G* value for 100 keV STEM-EELS derived from tabulated atomic cross sections[14] is 0.0057. The corresponding *G* value for C 1s NEXAFS is 100/285 = 0.35 (since each absorbed photon gives useful information). The figures of merit for comparing the two techniques on this basis are thus (1450 × 0.0057) = 8.3 for electrons and (12 000 × 0.35) = 4200 for photons. This says that, for an equal amount of damage generated, photons are about 500 times more effective than electrons at providing useful C 1s near-edge signal. Of course, if longer energy ranges are required (e.g., for elemental quantitation), then the *G* value for STEM-EELS will increase, making it relatively more favorable. Conversely, if a very narrow energy range suffices for a specific analysis, then the relative advantage of STXM-XAS increases.

An alternative perspective on the relative analytical capability can be obtained by evaluating the relative energy doses delivered in recording the first spectrum of each experimental damage series. The area exposed was a 100 μm^2 square for STEM-EELS and a 0.2 μm^2 area disk for STXM-XAS. The energy doses used to record the first spectrum shown in Figures 3 and

TABLE 4: Energies (eV) and Proposed Assignments of O 1s Spectral Features of PET and DMT

	energies (eV)						
	PET				1,4-DMT	assignment	
no	FY-XAS	EY-XAS	STXM	p-EELS	ISEELS	C═O	C−O
1[a]	(531.5)	(531.5)	(531.5)	(531.5)	531.5	$\pi^*_{C=O}$ (a)[b]	
2		533.8	533.9	534.0	534.0	$\pi^*_{C=O}$ (b)	$\pi^*_{C=O}$ (d)
3 sh		536.8	536.7	536.8	536.4	$\pi^*_{C=O,C=C}$ (c)	$\pi^*_{C=O}$ (e)
IP[c]					537.0	IP	
4	540.3	540.8	540.3	540.9	540.3	σ^*_{C-O}	
IP[c]					540.5		IP
5 sh	546	546	546	546	546	$\sigma^*_{C=O}$	

[a] Set to the value determined for the main π^* of DMT: ISEELS calibration: −3.9 eV relative to π^* of CO_2 (535.4 eV).[59] [b] Letters refer to EHMO core excitation orbital pictures presented in Figure 5. [c] Estimated from the IPs of related species.[53]

4 are

electrons

$$10\ \text{s}\cdot 0.38 \times 10^{-9}\ \text{A}\cdot 6 \times 10^{18}\ \text{e}^-/(\text{A s})\cdot 35\ \text{eV/e}^-)/$$
$$(130\ \text{nm}\cdot 10000\ \text{nm}\cdot 10000\ \text{nm}) \sim 61\ \text{eV nm}^{-3}$$
(about 4% of the critical energy dose)

photons

$$(60\ \text{s}\cdot 4 \times 10^5\ \text{photon/s}\cdot 300\ \text{eV/photon})/$$
$$(200\ \text{nm}\cdot 250\ \text{nm}\cdot 250\ \text{nm}\cdot \pi) \sim 180\ \text{eV nm}^{-3}$$
(about 2% of the critical energy dose)

Thus, the first spectrum recorded by each technique was acquired using <5% of the critical dose. The area analyzed with STXM-XAS was smaller by a factor of 500. The ability of STXM to use a similar level of radiation damage to record a meaningful spectrum from a much smaller area than STEM is directly related to the analytical advantage of X-rays documented by the figure of merit described above.

In general, a useful way to compare the analytical capability of two spectromicroscopy techniques is in terms of the minimum sample size for which analytically meaningful spectra can be acquired. Many of the desired polymer applications of STXM or STEM-EELS involve characterization of dispersed phases where it is necessary to be able to identify chemical composition (speciation) of small regions or interfaces with submicron spatial resolution. Studies of damage rates of homogeneous systems (pure or mixed systems) such as the present work allow one to anticipate the applicability of either technique to specific problems, in terms of both quality of spectra and critical dose information. As one reaches the critical dose limits for radiation damage in either technique, one approach to extend the analytical utility without sacrificing spatial resolution is to sum spectra recorded for suitably brief periods over many identical particles. This can be done efficiently using a "mask" defined by an image recorded under low-damage conditions (e.g., an elastic image in STEM-EELS).[35] The actual minimum sample size achievable in either technique will depend on the desired energy range, energy resolution, and statistical precision. This comparative study of PET suggests that, when one takes into account the relevant factors, there is a difference of about 2 orders of magnitude between the two techniques in terms of the limitations imposed by radiation damage. This is in agreement with other published estimates.[22]

3.3. Spectral Assignments. *3.3.1. Carbon 1s Spectra of PET.* The energies and proposed assignments for the C 1s spectral features are summarized in Table 3. These assignments are guided by our earlier study of an extensive set of molecular analogue species,[18] as well as extended Hückel calculations of DMT.[18,52] The detailed assignments of the 284−287 eV features

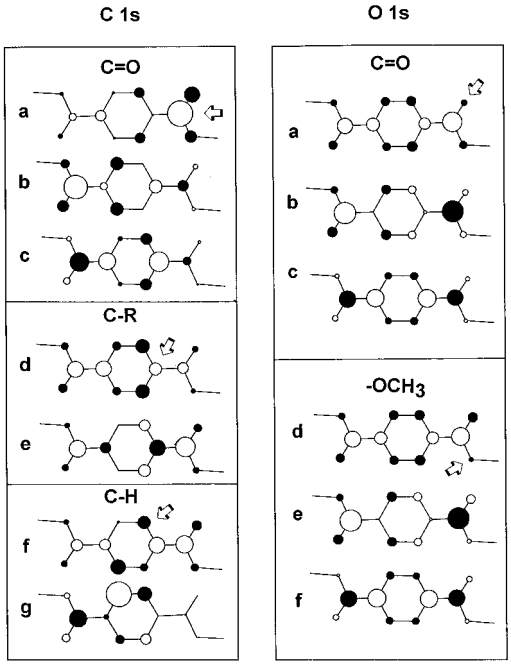

Figure 5. (left panel) Orbital diagrams of the upper levels of the most intense C 1s → π^* transitions derived from extended Hückel (EHMO-EICVOM) calculations. The arrow indicates the core excitation site. (right panel) EHMO orbital diagrams of the upper levels of the most intense O 1s → π^* transitions.

(nominally $\pi^*_{C=C}$) and the 288−290 eV features (nominally $\pi^*_{C=O}$) are of particular interest since these features give insight into electronic delocalization. Also these are the features which reflect orientation and phase dependent effects.[9] While one can attribute the lower energy π^* features to MOs of dominant $\pi^*_{C=C}$ character and the higher energy π^* features to MOs of dominant $\pi^*_{C=O}$ character, in fact there are strong interactions among the ring and carbonyl π^* levels such that the final state of the transitions actually have a mixed character. In addition, the nature of these interactions changes with location of the core hole. The EHMO calculations predict the orbital splitting caused by interactions of the $\pi^*_{C=O}$ and $\pi^*_{C=C}$ orbitals, as well as variations in molecular orbital character with variation in core hole position.

The results of EHMO calculations relating to the C 1s and O 1s spectra of DMT are presented in Figure 5. The EHMO predictions of the C 1s and O 1s spectra have been presented earlier, in comparison to STEM-EELS spectra of PET.[18] (Note that although the geometry employed in the earlier work differs slightly from that used in this study, the final spectral predictions are very similar.) Here we present pictures of the molecular orbitals in order to complement the earlier work by investigating the extent of delocalization in core excitation at each distinct site. The MO sketches show the contributions of each $2p_z(\pi)$

atomic orbital to the molecular orbital in the presence of the indicated core hole. Focusing first on excitations at the C−H ring carbons, EHMO predicts two main transitions separated by 1.2 eV, which are excitations to the orbitals depicted as (f, g) in Figure 5. These are C 1s(C−H) excitations to π^* orbitals of mixed $\pi^*_{C=C}$ and $\pi^*_{C=O}$ character. They make up the majority of the intensity of the lowest energy π^* band in the experimental spectra (Figure 1). The splitting of the transitions associated with C 1s(C−H) excitation to orbitals f and g has been resolved in small molecule analogues of PET,[18] it is clearly detected in the transmission XAS spectrum, and it shows up as the shoulder at 285.6 eV in the EY-XAS and ISEELS spectra. The EHMO calculated value of 1.2 eV is somewhat larger than the observed separation of 0.7 eV.

Focusing next on excitations at the C−R ring carbons (those to which the methyl carboxylate groups are attached), there are two low-lying π^* components (d, e) with a mixed $\pi^*_{C=C}$ and $\pi^*_{C=O}$ character and with an even larger separation (∼3 eV) than the (f, g) pair for C 1s(C−H) excitation. This large splitting, combined with the estimated ∼0.5 eV chemical shift between the C 1s(C−H) and C 1s(C−R) IPs,[53,54] places the first C 1s → $\pi^*_{C=C}/\pi^*_{C=O}$ transition (d) as part of the shoulder at 285.6 eV and the higher energy C 1s(C−R) → π^* transition (e) at the leading edge of the 288 eV peak, where a shoulder is observed in the highest resolution XAS spectrum of PET as well as the ISEELS of DMT. This large splitting arises from a combination of the effect of symmetry reduction on the degenerate e_{1u} orbital in benzene and the interaction of the $\pi^*_{C=C}$ and $\pi^*_{C=O}$ components. The delocalization interaction results in considerable mixing of excited state character which can generate a sizable splitting.

The third important aspect of the low-lying π^* structure arises from excitations at the C 1s(C═O) carbon. Here three π^* components (a−c) can be identified. The intense lowest energy component (a) corresponds to excitation to a $\pi^*_{C=O}$ orbital which is quite localized on the C 1s excited carbonyl, but which otherwise is an in-phase combination of the $\pi^*_{C=O}$ orbitals on the two methyl carboxylate groups (denoted $\pi^*_{C=O}(+)$ in ref 18). The next two components (b, c) are considerably weaker and of more mixed $\pi^*_{C=C}$ and $\pi^*_{C=O}$ character. Peak b is the out-of-phase $\pi^*_{C=O}$ combination (denoted $\pi^*_{C=O}(-)$ in ref 18) while the third component (c) is very much delocalized over both the ring and carbonyl groups. Based on the alignment with the experimental spectrum, EHMO predicts that the (a), (e), and (b) components produce the three peaks at 288, 289, and 290 eV. Understanding the identity of these structures is important since the 288−290 eV region is the region which differs the most between the polymer and monomer. Also, this is the spectral region which is most readily affected by radiation damage. It is possible there could be a connection between the spatial distribution of the initial excitation and the subsequent bond breaking.[55]

3.3.2. Oxygen 1s Spectra of PET. The energies and tentative assignments of the O 1s spectral features of PET are summarized in Table 4. The main π^* peak at 531.5 eV is attributed to O 1s(C═O) → $\pi^*_{C=O}(+)$ while the second peak at 534.0 eV is attributed to O 1s(C═O) → $\pi^*_{C=O}(-)$ and O 1s(C-O) → $\pi^*_{C=O}(+)$ transitions. The peak at 536.4 eV is attributed to O 1s(C-O) → $\pi^*_{C=O}(-)$ transitions. Some contributions of O 1s → Rydberg transitions may also exist between 534 and 540 eV in the ISEELS spectrum of gaseous DMT. However, these are generally expected to be rather weak in a molecule as large as DMT and are most likely absent in the spectrum of a polymer (but for a contrary viewpoint, see ref 56). The broad, intense peak at 540.8 eV is ascribed to O 1s (C−O) → σ^*_{C-O} transitions. There is also a broad, weak feature centered at about 547 eV. This is seen clearly in the ISEELS spectra of DMT, and it can be identified in most of the O 1s spectra of PET, with varying degrees of visibility (Figure 2). This broad signal is assigned to O 1s(C═O) → $\sigma^*_{C=O}$ transitions. The weak intensity of $\sigma^*_{C=O}$ relative to σ^*_{C-O} resonances has been noted in previous studies of the core spectra of ester species.[18,57]

The EHMO results generally support this interpretation of the O 1s spectrum of DMT. They predict there is extensive delocalization such that the final states of O 1s excitation at both the carbonyl and ether oxygen involve excitation to mixed $\pi^*_{C=C}/\pi^*_{C=O}$ orbitals as presented in Figure 5. The three π^* orbitals are rather similar for O 1s(C═O) (a−c) and O 1s(C−O) (d−f), although excitations from O 1s(C═O) are more intense than those from O 1s(C−O), as expected. The predicted splittings are almost 2 eV between each of the three components, which is somewhat smaller than that observed experimentally. Further discussion of the core spectra of 1,4-DMT is presented elsewhere, in the context of a comparison of the spectra and *ab initio* calculations of 1,2-, 1,3-, and 1,4-dimethyl phthalate isomers and their corresponding oligimers.[58]

4. Summary

The C 1s and O 1s spectra of poly(ethylene terephthalate) have been recorded by several techniques and have been compared to the spectra of the corresponding monomer (1,4-DMT). Once resolution differences have been taken into account, all of the polymer spectra recorded under low-dose conditions are generally in good agreement. This work demonstrates that, with a sufficiently high-performance system, STEM-EELS and STXM-XAS spectra of a relatively radiation sensitive polymer can be obtained with reasonable resolution and statistical precision before substantial radiation damage has occurred. Radiation damage was shown to be inducible by both electron and X-ray techniques, but it was also shown that spectra unaffected by damage could be acquired by both techniques. The quantitative analysis of the radiation damage rates produced a figure of merit indicating there is an ∼500-fold advantage of STXM-XAS analysis of room-temperature PET relative to STEM-EELS of cryocooled PET. NEXAFS, particularly the high-resolution STXM-XAS spectra, confirmed the splitting of the C 1s(C═O) → $\pi^*_{C=O}$ transitions predicted by earlier experimental studies and calculations of related systems,[18] and provided information as to the damage mechanism.

Acknowledgment. This work was supported in part by NSERC (Canada). The authors acknowledge the fine sample preparation work of G. Young at Dow and the assistance of S. Sun at NIH. We also thank Dow co-workers, B. DeKoven for assistance with the synchrotron runs, and J. Allen, C. Bosnyak, and R. Woods for help with the PET preparation. The authors are indebted for the assistance of J. Hunt (Lehigh University) with the low-dose polymer EELS measurements. We thank J. Kirz and C. Jacobsen and their groups for the development and maintenance of the X1A-STXM at NSLS. The zone plates utilized in the NSLS and ALS STXMs were provided through an IBM-LBL collaboration between E. Anderson, D. Attwood, and D. Kern. Parts of this work were performed at the NSLS and the ALS, which are supported by the Department of Energy, Office of Basic Energy Sciences. H.A. gratefully acknowledges an NSF Young Investigator Award (DMR-9458060) and support from Dow Chemical.

References and Notes

(1) Outka, D. A.; Stöhr, J. *Springer Ser. Surf. Sci.* **1989**, *109*, 201.

(2) Jordan-Sweet, J. L.; Kovac, C. A.; Goldberg, M. J.; Morar, J. F. *J. Chem. Phys.* **1989**, *89*, 2482.
(3) Ohta, T.; Seki, K.; Yokoyama, T.; Morisada, I.; Edamatsu, K. *Phys. Scr.* **1990**, *41*, 150.
(4) Castner, D. G.; Lewis, K. B.; Fischer, D. A.; Ratner, B. D.; Gland, J. L. *Langmuir*, **1993**, *9*, 537.
(5) Stöhr, J. *NEXAFS Spectroscopy*, Springer Series in Surface Science No. 25; Springer-Verlag: Berlin), 1992.
(6) Kirz, J.; Jacobsen, C.; Howells, M. *Q. Rev. Biophys.* **1995**, *33*, 33.
(7) Fischer, D. A.; Moodenbaugh, A. R.; Xu, Y. *Physica C* **1993**, *215*, 279.
(8) Leapman, R.; Grunes, L.; Fejes, P. L. *Phys. Rev. B* **1982**, *26*. 614; Leapman, R. D.; Silcox, J. *Phys. Rev. Lett.* **1979**, *42*, 1361.
(9) (a) Ouchi, I.; Nakai, I.; Kamada, M.; Tanaka, S.; Hagiwara, T. *Polym. J.* **1995**, *2*, 127. (b) Lippitz, A.; Friedrich, J. F.; Unger, W. E. S.; Schertel, A.; Wöll, Ch. *Polymer* **1996**, *37*, 3151.
(10) Ade, H.; Zhang, X.; Cameron, S.; Costello, C.; Kirz, J.; Williams, S. *Science*, **1992**, *258*, 972.
(11) Ade, H.; Hsiao, B. *Science* **1993**, *262*, 1427.
(12) Hitchcock, A. P. *Phys. Scr.* **1990**, T*31*, 159.
(13) Sze, K. H.; Brion, C. E. *J. Electron Spectrosc.* **1991**, *57*, 117. Sze, K. H.; Brion, C. E. *Chem. Phys. Lett.* **1989**, *137*, 353.
(14) Egerton, R. F. *Electron Energy Loss Spectroscopy in the Electron Microscope*; Plenum Press: New York, 1986.
(15) Hofer, F.; Geymeyer, W. R.; Ingolic, E. Proceedings of the XI International Congress on Electron Microscopy, Kyoto, 1986.
(16) Krivanek, O. L. *EMSA Bulletin*, **1988**, *18*, 65.
(17) Rightor, E. G.; Young, G. P.; Urquhart, S. G.; Hitchcock, A. P. *Microscopy The Key Reseach Tool* **1992**, *22*, 67.
(18) Hitchcock, A. P.; Urquhart, S. G.; Rightor, E. G. *J. Phys. Chem.* **1992**, *96*, 8736.
(19) Urquhart, S. G.; Hitchcock, A. P.; Rightor, E. G.; Priester, R. D.; Leapman, R. D. *J. Polym. Sci. B Polym. Phys.* **1995**, *33*, 1593.
(20) Blackson, J. H.; Susnitzky, D. W.; Beaman, D. R. *Proc. 52nd MSA Meetin*g **1994**, 946.
(21) Urquhart, S. G.; Hitchcock, A. P.; Rightor, E. G.; Priester, R. D. *J. Polymer Sci. B Polym. Phys.* **1995**, *33*, 1603.
(22) Isaacson, M.; Utlaut, M. *Optik* **1978**, *50*, 213. Isaacson, M. S. In *Principles and Techniques of Electron Microscopy*; Hayat, M., Ed.; Van Nostrand-Reinhold: New York, 1977; Vol. 7.
(23) Egerton, R. F.; Crozier, P. A.; Rice, P. *Ultramicroscopy* **1987**, *23*, 305.
(24) Ciliax, B. J.; Kirk, K. L.; Leapman, R. D. *Ultramicroscopy* **1993**, *48*, 13.
(25) Zaera, F.; Fischer, D. A.; Shen, S.; Gland, J. L. *Surf. Sci.* **1988**, *194*, 205.
(26) Fischer, D. A.; Colbert, J.; Gland, J. L. *Rev. Sci. Instrum* **1989**, *60*, 1596.
(27) Jacobsen, C.; Williams, S.; Anderson, E.; Brown, M. T.; Buckley, C. J.; Kern, D.; Kirz, J.; Rivers, M.; Zhang, X. *Opt. Commun.* **1991**, *86*, 351. Zhang, X.; Jacobsen, C.; Williams, S. In *Soft X-ray Microscopy*; Jacobsen, C.; Trebes, J., Eds.; *Proc. SPIE* **1992**, *1741*, 251.
(28) Kirz, J.; Ade, H.; Howells, M.; Jacobsen, C.; Ko, C.−H.; Lindaas, S.; McNulty, I.; Sayre, D.; Williams, S.; Zhang, X. *Rev. Sci. Instrum.* **1992**, *63*, 557.
(29) Padmore, H. A.; Warwick, T. *J. Synchrotron Rad.* **1994**, *1*, 27. Warwick, T.; Ade, A.; Hitchcock, A. P.; Padmore, H. A.; Rightor, E. G.; Tonner, B. P. *J. Electron Spectrosc.*, submitted.
(30) Ma, Y.; Chen, C. T. ; Meigs, G.; Randall, K.; Sette, F. *Phys. Rev. A* **1991**, *44*, 1848.
(31) Hitchcock, A. P.; Mancini, D. C. *J. Electron Spectrosc.* **1994**, *33*, 1.
(32) Henke, B. L.; Lee, P.; Tanaka, T. J.; Shimabukuro, R. L.; Fujikawa, B. K. *At. Data Nucl. Data Tables* **1982**, *27*, 1.
(33) Krivanek. O. L.; Ahn, C. C.; Keeney, R. B. *Ultramicroscopy* **1987**, *22*, 103. Krivanek, O. L.; Paterson, J. H.; Poppa, H. R. *Proc. 47th EMSA* **1989**, p 410.
(34) Leapman, R. D.; Andrews, S. B. *J. Microsc.* **1991**, *161*, 3.
(35) Hunt, J. A.; Leapman, R. D.; Williams, D. B. *Proc. 27th MBAS* **1993**, *2*, 272.
(36) Leapman, R. D.; Fiori, C. I.; Swyt, C. R. *J. Microsc.* **1984**, *133*, 239.
(37) Leapman, R. D. In *Transmission Electron Energy Loss Spectroscopy in Materials Science*; Disko, M. M., Ahn, C. C., Fultz, B., Eds.; 1992; p 47.
(38) Howell, J.; Rossi, A.; Wallace, D.; Haraki, K.; Hoffmann, R. FORTICON8 Program QCMP011 from Quantum Chemistry Program Exchange, Creative Arts Bldg, Indiana University, Bloomington, IN 47404.
(39) Mealli, C.; Proserpio, D. M. *J. Chem. Educ.* **1990**, *67*, 339.
(40) Brisse, P. F.; Pérez, S. *Acta Crystallogr. B* **1976**, *32*, 2110.
(41) Rühl, E.; Hitchcock, A. P. *J. Am. Chem. Soc.* **1989**, *111*, 5069.
(42) Rühl, E.; Wen, A. T.; Hitchcock, A. P. *J. Electron Spectrosc.* **1991**, *57*, 137.
(43) Wen, A. T.; Rühl, E.; Hitchcock, A. P. *Organometallics* **1992**, *11*, 2559.
(44) Francis, J. T.; Hitchcock, A. P. *J. Phys. Chem.* **1992**, *96*, 6598.
(45) Schwarz, W. H. E. *Chem. Phys.* **1975**, *11*, 217.
(46) Egerton, R. E.; Crozier, P. A.; Rice, P. *Ultramicroscopy* **1987**, *23*, 305.
(47) Kumar, S.; Adams, W. W. *Polymer* **1990**, *31*, 15.
(48) Payne, R. S.; Beamson, G. *Polymer* **1993**, *34*, 1637.
(49) Zhang, X.; Jacobsen, C.; Lindaas, S.; and Williams, S. *J. Vac. Sci. Technol. B* **1995**, *13*, 1477.
(50) Tinone, M. C. K., Tanaka, K.; Ueno, N. *J. Vac. Sci. Technol. A* **1995**, *13*, 1885.
(51) Wollersheim, O.; Zumaqué, H.; Hormes, J.; Kadereit, D.; Langen, J.; Haussling, L.; Hoessel, P.; Hoffmann, G. *Nucl. Instrum. Methods B* **1995**, *97*, 273.
(52) Urquhart, S. G.; Hitchcock, A. P.; Rightor, E. G.; Smith, P. A.; Ade, H. *Proc. Mater. Res. Soc.*, in press.
(53) Jolly, W. L.; Bomben, K. D.; Eyermann, C. J. *At. Data Nucl. Data Tables* **1984**, *31*, 109.
(54) Beamson, G.; Briggs, D. *High Resolution XPS of Organic Polymers: The Scienta ESCA300 Database*; Wiley: New York, 1992. The narrowest line in their XPS spectrum of PET is 0.85 eV fwhm (C 1s(C═O)) whereas the C 1s(ring) peak is 1.0 eV wide. Two 0.85 eV peaks separated by 0.5 eV in a 2:1 ratio gives a near symmetric peak 1.0 eV in width. From this we conclude that the C 1s(C−R) IP is ∼0.5 eV above the C 1s(C−H) IP. A lower resolution XPS spectrum of PET, along with a discussion of the dependence of the XPS on conformation, is given in: Boulanger, P.; Pireaux, J. J.; Berbist, J. J.; Delhalle, J. *J. Electron Spectrosc.* **1993**, *63*, 53.
(55) Hanson, D. M. *Adv. Chem. Phys.* **1990**, *77*, 1.
(56) Bagus, P. S.; Weiss, K.; Schertel, A.; Wöll, Ch.; Braun, W.; Hellwig, C.; Jung, C. *Chem. Phys. Lett.* **1996**, *248*, 129.
(57) Ishii, I.; Hitchcock, A. P. *J. Electron Spectrosc.* **1987**, *46*, 55.
(58) Urquhart, S. G.; Hitchcock, A. P.; Smith, A. P.; Ade, H.; Rightor, E. G. *J. Phys. Chem.*, in press.
(59) Sodhi, R. N. S.; Brion, C. E. B. *J. Electron Spectrosc.* **1984**, *34*, 363.